Energetics and proton release in photosystem II from Thermosynechococcus elongatus with a D1 protein encoded by either the psbA or psbA gene

Alain Boussac, Julien Sellés, Miwa Sugiura

Energetics and proton release in Photosystem II from *Thermosynechococcus elongatus* with a D1 protein encoded by either the *psbA*$_2$ or *psbA*$_3$ gene.

Alain Boussac[1*], Julien Sellés[2], Miwa Sugiura[3],

[1] I^{2}BC, UMR CNRS 9198, CEA Saclay, 91191 Gif-sur-Yvette, France.

[2] Institut de Biologie Physico-Chimique, UMR CNRS 7141 and Sorbonne Université, 13 rue Pierre et Marie Curie, 75005 Paris, France.

[3] Proteo-Science Research Center, and Department of Chemistry, Graduate School of Science and Technology, Ehime University, Bunkyo-cho, Matsuyama, Ehime 790-8577, Japan.

*Corresponding authors: alain.boussac@cea.fr

The authors declare that they have no conflict of interest.

ORCID numbers:

Alain Boussac: 0000-0002-3441-3861

Julien Sellés: 0000-0001-9262-8257

Abbreviations:

Chl, chlorophyll; PSII, Photosystem II; MES, 2–(*N*–morpholino) ethanesulfonic acid; P_{680}, primary electron donor; P_{D1} and P_{D2}; Chl monomer of P_{680} on the D1 or D2 side, respectively; Phe_{D1} and Phe_{D2}, pheophytin on the D1 and D2 side, respectively; Q_A, primary quinone acceptor; Q_B, secondary quinone acceptor; Tyr_Z, redox active tyrosine 161 of D1; WT*1,2,3 *T. elongatus* mutant strain containing only the *psbA*$_{1,2,3}$ gene, respectively, and a His_6-tag on the C-terminus of CP43; EPR spectroscopy, Electron Paramagnetic Resonance spectroscopy; TL, thermoluminescence; PPBQ, phenyl *p*–benzoquinone; DCMU, 3-(3,4-dichlorophenyl)-1,1-dimethylurea; E_m, redox potential *versus* normal hydrogen electrode (NHE).

Abstract

In the cyanobacterium *Thermosynechococcus elongatus*, there are three *psbA* genes coding for the Photosystem II (PSII) D1 subunit that interacts with most of the main cofactors involved in the electron transfers. Recently, the 3D crystal structures of both PsbA2-PSII and PsbA3-PSII have been solved [Nakajima et al., J. Biol. Chem. 298 (2022) 102668.]. It was proposed that the loss of one hydrogen bond of Phe_{D1} due to the D1-Y147F exchange in PsbA2-PSII resulted in a more negative E_m of Phe_{D1} in PsbA2-PSII when compared to PsbA3-PSII. In addition, the loss of two water molecules in the Cl-1 channel was attributed to the D1-P173M substitution in PsbA2-PSII. This exchange, by narrowing the Cl-1 proton channel, could be at the origin of a slowing down of the proton release. Here, we have continued the characterization of PsbA2-PSII by measuring the thermoluminescence from the $S_2Q_A^-$/DCMU charge recombination and by measuring proton release kinetics using time-resolved absorption changes of the dye bromocresol purple. It was found that *i*) the E_m of $Phe_{D1}^{-\bullet}/Phe_{D1}$ was decreased by ~ 30 mV in PsbA2-PSII when compared to PsbA3-PSII and *ii*) the kinetics of the proton release into the bulk was significantly slowed down in PsbA2-PSII in the $S_2Tyr_Z^\bullet$ to S_3Tyr_Z and $S_3Tyr_Z^\bullet \rightarrow (S_3Tyr_Z^\bullet)$' transitions. This slowing down was partially reversed by the PsbA2/M173P mutation and induced by the PsbA3/P173M mutation thus confirming a role of the D1-173 residue in the egress of protons trough the Cl-1 channel.

Introduction

The water splitting by Photosystem II (PSII) in plants, cyanobacteria, and algae produces the atmospheric dioxygen. PSII consists of 17 trans-membrane proteins and 3 to 5 extrinsic membrane proteins depending on the species [1-4]. The mature PSII binds 35 chlorophylls *a* (Chl-*a*), 2 pheophytins (Phe), 1 membrane b-type cytochrome, 1 extrinsic c-type cytochrome (in cyanobacteria and red algae), 1 non-heme iron, 2 plastoquinones (Q_A and Q_B), the Mn_4CaO_5 cluster, 2 Cl^-, 12 carotenoids and 25 lipids. In the cyanobacterium *Synechocystis* sp. PCC 6803 a 4th extrinsic subunit, PsbQ, has also been found in addition to PsbV, PsbO and PsbU [3].

Among the 35 Chl-*a*, 31 are antenna Chls. After the absorption of a photon by these antenna Chls, the excitation energy is transferred to the photochemical trap that consists of the four Chls; P_{D1}, P_{D2}, Chl_{D1}, Chl_{D2}. These 4 Chls, together with the 2 Phe molecules, Phe_{D1} and Phe_{D2}, constitute the reaction center of PSII. A few picoseconds after the formation of the excited Chl_{D1}^*, a charge separation occurs resulting ultimately in the formation of the $Chl_{D1}^+Phe_{D1}^-$ and then $P_{D1}^+Phe_{D1}^-$ radical pair states [5,6]. After this charge separation, P_{D1}^+ oxidizes Tyr_Z, the Tyr161 of the D1 polypeptide, which then is reduced by the Mn_4CaO_5 cluster. The electron on Phe_{D1}^- is then transferred to Q_A, the primary quinone electron acceptor, and then to Q_B, the second quinone electron acceptor. Whereas Q_A can be only singly reduced under normal conditions, Q_B accepts two electrons and two protons before to leave its binding site and to be replaced by an oxidized Q_B molecule from the membrane plastoquinone pool, see for example [7-11] for a non-exhaustive list of recent reviews on PSII function.

The Mn_4CaO_5 cluster, oxidized by the $Tyr_Z^\bullet$ radical formed after each charge separation, cycles through five redox states denoted S_n, where *n* stands for the number of stored oxidizing equivalents. The S_1-state is stable in the dark, which makes S_1 the preponderant state after dark-adaptation. When the S_4-state is formed, after the 3rd flash of light given on dark-adapted PSII, two water molecules bound to the cluster are oxidized, O_2 is released and the S_0-state is reformed, [12,13], see *e.g.* [7-9,14] for recent reviews on the Mn_4CaO_5 redox cycle.

The D1 and D2 proteins bear the main cofactors involved in electron transfer reactions. In the *T. elongatus* genome there are three different *psbA* genes encoding a D1 protein [15]. They are tlr1843 (*psbA*$_1$), tlr1844 (*psbA*$_2$) and tlr1477 (*psbA*$_3$). The amino acid sequences deduced from the *psbA* genes, among the 344 amino acids, points a difference of 21 residues between PsbA1 and PsbA3, 31 residues between PsbA1 and PsbA2, and 27 residues between

PsbA2 and PsbA3. Whereas the *psbA$_1$* and *psbA$_2$* genes are contiguous in the genome, with the initial codon of *psbA$_2$* located 312 bp downstream of the terminal codon of *psbA$_1$* the *psbA$_3$* gene is located independently and apart from *psbA$_1$* and *psbA$_2$*.

The presence of several *psbA* genes is a common feature in cyanobacteria and these genes are, at least partially, differentially expressed depending on the environmental conditions [16,17]. For example, under high light conditions, PsbA3 is predominantly produced [18] whereas the *psbA$_2$* transcript is up-regulated under either UV illumination [19] or under micro-aerobic conditions [20]. Some functional differences between PSII with either PsbA1, PsbA2, and PsbA3 have been already characterized and discussed [21-24]. The main findings are briefly summarized below.

The split EPR signal arising from the magnetic interaction between $Tyr_Z^{\bullet}$ and the cluster in the $(S_2Tyr_Z^{\bullet})'$ state, which is induced by near-infrared illumination at 4.2 K of the S_3Tyr_Z state, is significantly modified, and the slow phases of P_{680}^{+} reduction by Tyr_Z are slowed down from the hundreds of μs time range to the ms time range. These two results [21,24] were interpreted at that time by a change in the geometry of the Tyr_Z phenol and its environment, likely the Tyr-O…H…Nε-His bonding, in PsbA2-PSII when compared with PsbA(1/3)-PSII. They also pointed to the dynamics of the proton-coupled electron transfer processes associated with the oxidation of Tyr_Z being modified in PsbA2-PSII. From sequence comparison, we proposed that the C144P and P173M substitutions in PsbA2 *versus* PsbA(1/3), respectively located upstream of the α-helix bearing Tyr_Z and between the two α-helices bearing Tyr_Z and its hydrogen-bonded partner, His-190, were responsible for these changes.

From the observed similar $S_1Tyr_Z^{\bullet}Q_A^{-\bullet}$ charge recombination kinetics at 4.2 K in PsbA2-PSII and PsbA3-PSII we predicted that $E_m(Q_A/Q_A^{-\bullet})$ in PsbA2-PSII was similar to that in PsbA3-PSII [22].

When the *T. elongatus* genome has only the *psbA$_2$* gene for D1, a hemoprotein was found to be present in large amount in cells. This new hemoprotein was identified to be the *tll0287* gene product with a molecular mass close to 19 kDa. The overall structure of Tll0287 was found to be similar to some kinases and sensor proteins with a Per-Arnt-Sim-like domain rather than to other c-type cytochromes. The fifth and sixth axial ligands for the heme are Cys and His which results in a low E_m (~ -255 mV *vs* NHE). Possible functions of Tll0287 as a redox sensor under micro-aerobic conditions or a cytochrome subunit of an H_2S-oxidizing system were proposed taking into account the environmental conditions in which *psbA2* is expressed, as well as phylogenetic analysis, structural, and sequence homologies [23].

Interestingly, when the promotor of the *psbA*$_2$ gene in a *ΔpsbA*$_1$, *ΔpsbA*$_3$ deletion mutant is replaced by the promotor of *psbA*$_3$, Tll0287 is no longer produced at a level detectable by EPR in whole cells (Sugiura and Boussac, unpublished data) thus suggesting that the promotor of *psbA*$_2$ has a role in triggering the expression of Tll0287.

By studying PsbA3/Pro173Met and PsbA2/Met173Pro site-directed mutants we concluded that the Pro173Met substitution in PsbA2-PSII versus PsbA3-PSII was an important structural determinants of the functional differences between PsbA2-PSII and PsbA3-PSII. For example, in PsbA2-PSII and PsbA3/P173M-PSII, we found that the oxidation of Tyr_Z by $P_{680}^{+\bullet}$ was specifically slowed down during the transition between S-states associated with proton release. We thus proposed that the increase of the electrostatic charge of the Mn_4CaO_5 cluster in the S_2 and S_3 states could weaken the H-bond interaction between $Tyr_Z^{\bullet}$ and D1/His190 in PsbA2 versus PsbA3 and/or induce structural modification(s) of the water molecules around Tyr_Z [24].

Very recently, the PsbA2-PSII and PsbA3-PSII structures were solved at a 1.9 Å resolution [25]. Based on the longer distance modelled from the crystallographic data between Phe_{D1} and D1-Y126 and the loss of an H-bond due to the D1-Y147F substitution in PsbA2-PSII compared to PsbA3-PSII, a destabilization of Phe_{D1}^- was expected in PsbA2-PSII [25]. Consequently, the authors in [25] expected a more negative redox potential for Phe_{D1} in PsbA2-PSII than in both PsbA3-PSII and PsbA1-PSII. Part of the increase of the E*m* of Phe_{D1} from -522 mV in PsbA1-PSII to -505 mV in PsbA3-PSII [26-28] has been explained by a stronger hydrogen bond between Phe_{D1} and Glu130 of D1 in PsbA3-PSII when compared to PsbA1-PSII, *e.g.* [29], with Gln130 in D1.

Finally, the change of D1-Ser270 in PsbA1-PSII and PsbA2-PSII to D1-Ala270 in PsbA3-PSII results in the loss of a H-bond between D1-Ser270 and a sulfoquinovosyl-diacylglycerol molecule near Q_B. This may result in an easier exchange of bound Q_B with a free plastoquinone, hence an enhancement of oxygen evolution in PsbA3-PSII due to a higher Q_B exchange efficiency [25] as suggested earlier [21]. The fourth important observation was that two water molecules in the Cl-1 channel were lost in PsbA2-PSII due to the change of D1-P173M, leading to the narrowing of the channel. The authors in [25] concluded that by affecting the proton transfer this may explain the lower efficiency of the S-state transition beyond S_2 by delaying the P_{680}^+ reduction in the S_2 and S_3 states in PsbA2-PSII as observed in [26]. However, the changes in the environment of Tyr_Z predicted in [22,24] are likely too small to be detectable in the structures.

In this work, we have estimated the E*m* of Phe_{D1} in PsbA2-PSII from thermoluminescence measurements and the kinetics of the proton release by following the time-resolved absorption change of the dye bromocresol purple. We have also monitored the effect of the D1-P173M exchange in PsbA3PSII and the effect of the D1-M173P exchange in PsbA2-PSII. Fig. 1 shows some of the structural changes identified between PsbA2-PSII and PsbA3-PSII in [25] and discussed in the present work.

Materials and Methods

PSII samples used

The *T. elongatus* strains used in this study were; *i*) the *ΔpsbA₁, ΔpsbA₂* deletion mutant, called WT*3 [30], constructed from the *T. elongatus* 43-H strain that had a His_6-tag on the carboxy terminus of CP43 [31] and in which the D1 protein is PsbA3; *ii*) the *ΔpsbA₁, ΔpsbA₃* deletion mutant, called WT*2 [21], also constructed from the *T. elongatus* 43-H strain, and in which the D1 protein is PsbA2; *iii*) the PsbA3/P173M mutant constructed in WT*3 cells [24]; *iv*) the PsbA2/M173P mutant constructed in WT*2 cells [24]. PSII purification from these 4 strains was achieved as previously described [24]. For the measurements in the presence of bromocresol purple [32], the samples were washed by cycles of dilution in 1 M betaine, 15 mM $CaCl_2$, 15 mM $MgCl_2$, followed by concentration using Amicon Ultra-15 centrifugal filter units (cut-off 100 kDa) until the estimated residual Mes concentration was ≤ 1 µM in the concentrated PSII samples before the final dilution for the ΔI/I measurements.

Time-resolved absorption change spectroscopy

Time-resolved absorption changes measurements were done with a lab-built spectrophotometer [33] with the previously described modifications [34]. For the 440 nm-*minus*-424 nm [32,35] the PSII were diluted in a medium containing 1 M betaine, 15 mM $CaCl_2$, 15 mM $MgCl_2$, 40 mM MES at pH 6.3 (adjusted with NaOH). For the measurements aimed at following the absorption changes of bromocresol purple at 575 nm the samples were diluted in a medium containing 1 M betaine, 15 mM $CaCl_2$, 15 mM $MgCl_2$, and 150 µM bromocresol purple. PSII samples were dark-adapted for ~ 1 h at room temperature (20–22°C) before to be diluted at 25 µg Chl/mL then, 100 µM phenyl *p*–benzoquinone (PPBQ) dissolved in dimethyl sulfoxide were added for the two measurements. In addition, for the proton

release/uptake measurements, 100 µM ferricyanide from a stock solution, adjusted to pH 6.3 prior to its addition, was also added to avoid contributions from the 2 $PPBQ^-$ + 2 H^+ → $PPBQH_2$ + PPBQ reaction. After the ΔI/I measurements, the absorption of each diluted batch of samples was precisely controlled to avoid errors due to the dilution of concentrated samples. The ΔI/I values were then normalized to A_{673} = 1.75 [32,35].

Thermoluminescence measurements

Thermoluminescence (TL) curves were measured with a lab-built apparatus [36,37]. PSII samples were diluted in 1 M betaine, 40 mM MES, 15 mM $MgCl_2$, 15 mM $CaCl_2$, pH 6.5 and then dark-adapted for at least 1 h at room temperature. Flash illumination was done at -10°C by using a saturating xenon flash. The constant heating rate was 0.4°C/s. After the dilutions of the PSII samples, and before the dark adaptation, the OD was precisely adjusted to 0.70 at 673 nm (*i.e.* ~ 10 µg Chl/mL). For the $S_2Q_A^-$/DCMU charge recombination, the DCMU (10 µM final concentration) dissolved in ethanol was added before loading the sample into the TL cuvette.

Results

Kinetics of the S-state dependent proton release.

Fig. 2 shows the kinetics of the absorption changes of bromocresol purple at pH 6.3 with PsbA3-PSII (Panel A), same data as in [38], PsbA2-PSII (Panel B), PsbA3/P173M-PSII (Panel C), and PsbA2/M173P-PSII (Panel D). The measurements were done after the 1st (black points), the 2nd (red points), the 3rd (blue points) and the 4th (green points) laser flashes given on dark-adapted PSII. The analysis of the results in PsbA3-PSII (Fig. 2A) has been previously done in detail [32,38], see also [39] for comparable data in Plant PSII. It is, however, briefly summarized in the next paragraph before to describe the data in the three other samples.

In Fig. 2A, the slow increase in the ΔI/I starting at ~ 100 µs after the flash, and clearly detectable after the first flash in PsbA3-PSII because there is no proton release in the $S_1Tyr_Z^\bullet$ to S_2Tyr_Z transition, corresponds to the proton uptake with a $t_{1/2}$ close to 300 µs (Table 1) occurring *after* the reduction of the oxidized non-heme iron by Q_A^- that have a $t_{1/2}$ ~ 50 µs [40].

After the second flash, mainly in the $S_2Tyr_Z^{\bullet}$ to S_3Tyr_Z transition, a proton release occurred with a $t_{1/2}$ close to ~ 50 µs. After the third flash, a biphasic kinetics was resolved for the proton release. The fastest phase decayed with a $t_{1/2}$ of ~ 30 µs and the slowest one decayed with $t_{1/2}$ ~ 1.9 ms. These two phases in the proton release corresponds to the two steps in the $S_3Tyr_Z^{\bullet} \rightarrow (S_3Tyr_Z^{\bullet})' \rightarrow S_0Tyr_Z$ transitions, *e.g.* [39]. After the 4th flash, *i.e.* in the $S_0Tyr_Z^{\bullet}$ to S_1Tyr_Z transition, a proton release occurred with a $t_{1/2}$ ~ 200 µs.

For the longest times, a slow drift was observed after all the flashes. It likely includes the end of the proton uptake due to the reduction of the oxidized non-heme iron. This drift does not significantly perturb the interpretation of the kinetics before 1 ms. For example, in this time range, it is clear that the amplitude of the absorption changes are comparable in the $S_2Tyr_Z^{\bullet}$ to S_3Tyr_Z, $S_0Tyr_Z^{\bullet}$ to S_1Tyr_Z and $S_3Tyr_Z^{\bullet} \rightarrow (S_3Tyr_Z^{\bullet})'$ transitions. However, the drift may slightly decrease the amplitude of the slower phase in the S_3 to S_0 transition, see [32] for a discussion on this point. In the $S_2Tyr_Z^{\bullet} \rightarrow S_3Tyr_Z$ transition the proton release precedes the oxidation of the Mn_4CaO_5 cluster. In the $S_0Tyr_Z^{\bullet}$ to S_1Tyr_Z transition the proton release is approximately 4 times slower than the oxidation of the Mn_4CaO_5 cluster by $Tyr_Z^{\bullet}$ [32,39]. A proton release occurs in the first of the two $S_3Tyr_Z^{\bullet} \rightarrow (S_3Tyr_Z^{\bullet})' \rightarrow S_0Tyr_Z$ transitions whereas the release of the second proton is concomitant to the O_2 production. The results of the fits are listed in Table 1.

In PsbA2-PSII, PsbA3/P173M-PSII and PsbA2/M173P-PSII (Fig. 2B,2C,2D), the very small decay in the ΔI/I observed after the 1st flash (black points) could be indicative of a proton release in the $S_1Tyr_Z^{\bullet}$ to S_2Tyr_Z transition in contrast to the situation in PsbA3-PSII. Alternatively, and most likely, this proton release could occur in a very small fraction (≤ 10 %) of PsbA2-PSII would have been damaged during the washings because the $t_{1/2}$ is very close to that measured in Mn-depleted PSII in which the $t_{1/2}$ is ~ 10-20 µs (not shown), *i.e.* in the same time range as the oxidation of Tyr_Z by $P_{680}^{+\bullet}$ [41].

In PsbA2-PSII, after the second flash (red points), the main decay kinetics had a $t_{1/2}$ ~ 100 µs. Clearly, the proton release in the $S_2Tyr_Z^{\bullet} \rightarrow S_3Tyr_Z$ transition is twice as slow as in the PsbA3-PSII. After the third flash (blue points), the slow phase associated to the O_2 evolution had a similar $t_{1/2}$ (~ 1.9-1.6 ms) in PsbA3-PSII and PsbA2-PSII. In contrast, the fast phase with a $t_{1/2}$ ~ 80 µs was two to three times slower than in PsbA3-PSII. The situation after the fourth flash (green points) is more delicate to interpret because the miss parameter in PsbA2-PSII is larger than in PsbA3-PSII [21]. Consequently, there is a higher contribution of the $S_3Tyr_Z^{\bullet} \rightarrow (S_3Tyr_Z^{\bullet})' \rightarrow S_0Tyr_Z$ transitions after the fourth flash. This is particularly clear

with the presence of $t_{1/2}$ ~ 1.9 ms phase corresponding to the $(S_3Tyr_Z^{\bullet})' \rightarrow S_0Tyr_Z$ transition. Nevertheless this complication, the phase with a half time of 200 µs seems to be absent and replaced by a kinetics with a half time of ~ 90-100 µs. That could suggest that in the $S_0Tyr_Z^{\bullet}$ to S_1Tyr_Z transition, the proton release in PsbA2-PSII would be more than twice as fast as in PsbA3-PSII.

Fig. 2C shows the flash dependent kinetics in PsbA3/P173M-PSII. The same question as in the PsbA2-PSII arises for the fast decay phase that has a larger amplitude than in PsbA2-PSII. After the second flash (red points), the proton release with $t_{1/2}$ ~ 80 µs was significantly faster than in PsbA3-PSII and almost similar to that in PsbA2-PSII. After the third flash (blue points), the slow phase for the proton release had $t_{1/2}$ close to 2.0 ms, a value close to that in the other samples taking into account the accuracy of the measurement. The fast phase had a $t_{1/2}$ ~ 90 µs, *i.e.* a value comparable to that in PsbA2-PSII and 3 times longer than that in PsbA3-PSII. After the fourth flash (green points) there was no evidence for a large 2.0 ms phase thus indicating a smaller miss parameter than in PsbA2-PSII. Instead, the decay is almost monophasic with a $t_{1/2}$ close to 100 µs that is 2 times faster than in PsbA3-PSII and close to the possible fast phase detected in PsbA2-PSII.

Fig. 2D shows the flash dependent kinetics in PsbA2/M173P-PSII and after the first flash (black points) the same comments as in PsbA2-PSII and PsbA3/P173M-PSII can be made. After the second flash (red points), the proton release occurred with $t_{1/2}$ ~ 50 µs that is a value very close to that in PsbA3-PSII and thus twice as fast as in PsbA2-PSII. After the third flash (blue points), the slow phase for the proton release had $t_{1/2}$ close to 1.7 ms, a value close to that in the other samples taking into account the accuracy of the measurement. The fast phase had a $t_{1/2}$ ~ 50 µs, *i.e.* a value faster than in PsbA2-PSII and intermediate between PsbA2-PSII and PsbA3-PSII. After the fourth flash (green points), although the global impression seems to suggest an acceleration of the proton release compared to PsbA2-PSII, the complexity of the trace and the number of points necessarily reduced in this kind of experiment does not allow us to conclude.

An additional observation concerns the kinetics for the proton uptake better detectable after the 1st flash. Nevertheless the small number of usable points it is quite clear that this kinetics is twice as slow in PsbA2-PSII than in PsbA3-PSII (Table 1) and that the P173M mutation in PsbA3 slowed down the uptake by a factor ~ 2 and the M173P mutation in PsbA2 accelerated the uptake also by a factor ~ 2.

Time-resolved absorption change differences 440 nm-minus-424 nm during the S-state cycle

The measurement of the 440 nm-*minus*-424 nm difference at various time after a flash is an alternative indirect method to probe the proton and electron transfer kinetics around P_{D1}. Indeed, the electrochromic band-shifts in the Soret region of the P_{D1} absorption spectrum at 440 nm takes into account both the proton uptake/release and the electron transfer events, *e.g.* [35,42] and references therein. For the removal of the contributions due to the reduction of Q_A the ΔI/I at 424 nm was also measured [42]. A detailed comparison of the measurement using bromocresol purple and the electrochromism 440 nm-*minus*-424 nm in PsbA3-PSII has been done recently [35] and only the main points useful to the present work will be reminded.

Fig. 3 shows the time-resolved absorption change differences 440 nm-*minus*-424 nm in PsbA3-PSII (Panel A) and in PsbA2-PSII (Panel B) after the first four flashes given on dark-adapted PSII. Whereas the kinetics between 5 µs and 10 µs are marred by a small artifactual response of bromocresol purple, discussed previously in [34,43], which makes the 5 µs point more or less unusable, this is not the case here and it can be plotted without any problem.

After the first flash (black points) the kinetics corresponds to the reduction of $Tyr_Z^{\bullet}$ by the Mn_4CaO_5 cluster, *i.e.* it corresponds to the $S_1Tyr_Z^{\bullet}$ to S_2Tyr_Z transition. This electron transfer reaction had a $t_{1/2}$ of ~ 15 µs in both the PsbA3-PSII (Panel A) and in PsbA2-PSII (Panel B).

After the second flash (red points), the kinetics are dramatically different in the two samples. In PsbA3-PSII (Panel A), the fast phase with a $t_{1/2}$ of ~ 15-20 µs has been identified as a proton movement in the presence of the $S_2Tyr_Z^{\bullet}$ state [35], see also [44,45]. This proton movement is likely related, directly or indirectly, to the proton release into the bulk and detected with bromocresol purple with $t_{1/2}$ ~ 50 µs. The slow phase with $t_{1/2}$ ~ 200 µs corresponds to the reduction of $Tyr_Z^{\bullet}$ in the $S_2Tyr_Z^{\bullet}$ to S_3Tyr_Z transition occurring after the fast proton movement. In PsbA2-PSII (Panel B), the fast phase is missing suggesting that both the proton movement and the electron transfer occur simultaneously with a $t_{1/2}$ ~ 200 µs.

After the third flash (blue points), the kinetics is biphasic in both the PsbA3-PSII and PsbA2-PSII. The slow phase has the same $t_{1/2}$ (~ 1.5 ms) in the two PSII and it corresponds to the $(S_3Tyr_Z^{\bullet})' \rightarrow S_0Tyr_Z$ transition. In contrast, in PsbA2-PSII the fast phase with $t_{1/2}$ ~ 30 µs is twice as slow as in PsbA3-PSII with $t_{1/2}$ ~ 10-15 µs that is in agreement with the slowing down of the release of the proton into the bulk in this transition in PsbA2-PSII (see above).

After the fourth flash (green points), the kinetics in PsbA3-PSII is also biphasic. By taking into account the kinetics for the release of the proton into the bulk it is clear that the fast phase with $t_{1/2}$ ~ 15-20 µs corresponds to the electron transfer reaction that precedes the proton release which occurs with $t_{1/2}$ ~ 200 µs in the $S_0Tyr_Z^{\bullet}$ to S_1Tyr_Z transition. In PsbA2-PSII, the kinetics exhibits 2 phases and possibly 3 phases. The larger miss parameter in this PSII makes the interpretation more difficult. However, if we normalize the amplitude of the two kinetics in the two samples (not shown), the $t_{1/2}$ of the fast phase appears similar in PsbA3-PSII and PsbA2-PSII thus suggesting that the electron transfer reaction rates are similar in the two PSII. In contrast, the slow phase seems slower in PsbA2-PSII with $t_{1/2}$ ~ 500 µs. The additional slow phase in PsbA2-PSII with a $t_{1/2}$ ~ 1.5 ms likely corresponds to the $(S_3Tyr_Z^{\bullet})' \rightarrow S_0Tyr_Z$ transition and this is very likely due to the larger miss parameter.

Thermoluminescence

Fig. 4 shows the TL signals corresponding to the $S_2Q_A^-$/DCMU charge recombination in PsbA3-II (black points), PsbA2-PSII (blue points), PsbA3/P173M-PSII (red points) and PsbA2/M173P-PSII (green points). The peak temperature in PsbA3-PSII at ~ 15°C was as expected in this sample, *e.g.* [34]. In PsbA2-PSII, the peak temperature was shifted by +12°C to ~ 27°C and the amplitude of the signal was increased by a factor 4.

In the PsbA3/P173M-PSII the changes in the TL, when compared to the PsbA3-PSII, were qualitatively similar to those observed in PsbA2-PSII. The peak temperature was shifted to 29-30°C but the amplitude was only increased by a factor of ~ 2 (instead of 4 in PsbA2-PSII). In the PsbA2/M173P-PSII the peak temperature was ~ 27°C, *i.e.* almost unchanged when compared to PSbA2-PSII. The amplitude was nevertheless reduced by a factor of 2 so that it remained twice that in the PsbA3-PSII.

Discussion

In previous studies on the properties of PSII depending on the nature of the PsbA [21,22,24] it was shown that in PsbA2-PSII the reduction of $P_{680}^{+\bullet}$ by Tyr_Z is slower than in PsbA3-PSIIin the S_2 to S_3 and S_3 to S_3' transitions, *i.e.* the steps in which a proton transfer/release occurs *before* the electron transfer from the $Mn_4CaO_{5/6}$ cluster to $Tyr_Z^{\bullet}$. This

slow-down was shown to be significantly either reverted in the PsbA2/M173P mutant and induced in the PsbA3/P173M mutant.

Significant progress has been made recently with the publication of 3D structural models of PsbA2-PSII and PsbA3-PSII with a 1.9 Å resolution [25]. Many computational and experimental studies have addressed the proton channels, *e.g.* [34,46-49], and it is established that the Cl-1 channel is involved in the egress of protons, see *e.g.* [50-53] for some recent experimental evidence. The structure of PsbA2-PSII revealed that with a methione instead of a proline at the position 173 in D1, two water molecules in the Cl-1 channel are lost due to a narrowing of this channel [25]. There is not yet a structure of the PsbA2/M173P-PSII and PsbA3/P173M-PSII, but it seems very likely that this exchange alone can explain the slowdown in PsbA2-PSII of the rates of the proton releases in the $S_2Tyr_Z^{\bullet}$ to S_3Tyr_Z and $S_3Tyr_Z^{\bullet}$ to $(S_3Tyr_Z^{\bullet})$' transitions. However, in the $(S_3Tyr_Z^{\bullet})$' to S_0Tyr_Z transition the kinetics of the proton release is hardly affected thus strongly suggesting that either the egress of the proton in this step occurs *via* a different route that is not kinetically modified in PsbA2-PSII *versus* PsbA3-PSII, or that the removal of this proton from the cluster is the limiting step. In the $S_0Tyr_Z^{\bullet}$ to S_1Tyr_Z transition, the data are more difficult to analyse. The most likely reason is the larger miss parameter in PsbA2-PSII and the mutants. However, the proton released in this transition seems to use a different egress pathway, *e.g.* [53]. Presently, it is proposed that this proton initially originates from either protonated O4 [54-56] or protonated O5 [54] or a water molecule bound to the terminal Mn [57], whereas in the S_2 to S_3 transition, the first step is a deprotonation of W1 with the proton moving onto Asp61, *e.g.* [57-60]. Computational analysis of the hydrogen bond network in the vicinity of the oxygen evolving complex show that the waters are highly interconnected with similar free energy for hydronium at all locations [48] and this could result in multiphasic kinetics.

On the first flash, in PsbA3-PSII, the $t_{1/2}$ of the proton uptake (~ 320 µs) is ~ 6 times slower than the electron transfer rate between Q_A^- and Fe^{3+} (~ 55 µs) [40]. Therefore, the slower proton uptake in PsbA2-PSII more likely reflects a change in the proton ingress rather a dramatic change in the electron transfer rate between Q_A^- and Fe^{3+}, a kinetic rate that nevertheless would remain to determine in PsbA2-PSII. The amino-acids whose pK_a values have been shown, either experimentally [61,62] or by computational approaches [63], to be tuned by the redox state of the non-heme iron, like the D1-E243, D1-E244, D1-H252 and D1-His215, are conserved in the 3 PsbA variants so that they are not involved in the differences observed between PsbA2-PSII and PsbA3-PSII. The structural changes around Q_B in PsbA2-

PSII [25] can indirectly affect the kinetics of the proton uptake upon the reduction of the non-heme iron by $Q_A^{-\bullet}$. However it is more difficult to explain why the loss of two water molecules in the Cl-1 channel may slow down this kinetics by a factor 2 since the M173P mutation in PsbA3 has the same effect as the PsbA3 to PsbA2 exchange. More experiments are therefore required to determine which amino-acids participate in the ingress/egress of the proton following the reduction/oxidation of the non-heme iron.

Both the magnetic coupling between the $Ty_Z^{\bullet}$ radical and the Mn_4CaO_5 cluster in the S_2 state and the W-band EPR spectrum of $Tyr_Z^{\bullet}$ in Mn-depleted PSII are modified in PsbA3-PSII, and these modifications have been found induced by the P173M mutation alone in PsbA3-PSII, and reverted by the M173P mutation alone in PsbA2-PSII. This seems to be in disagreement with the 3D structures that reveal no differences in the Tyr_Z environment in PsbA2-PSII and PsbA3-PSII. However, *i*) these structures are those with Tyr_Z and not with $Tyr_Z^{\bullet}$, and *ii*) the structural changes causing the differences observed in EPR are probably too small to be detectable in a structure even with a 1.9 Å resolution.

The second important difference between PsbA2-PSII and PsbA3-PSII deduced from the structure, *i.e.* the loss of one H-bond between Phe_{D1} and Y147 in PsbA2-PSII, is an expected lower E_m of Phe_{D1} in PsbA2-PSII than in PsbA3-PSII [25]. The TL data reported here for the first time in PsbA2-PSII indicate that the energy level of $S_2Q_A^-$/DCMU is lower in PsbA2-PSII than in PsbA3-PSII and/or the energy level of the $P_{680}^{+\bullet}Phe_{D1}^{-\bullet}$ state is higher in PsbA2-PSII than in PsbA3-PSII [64,65]. The increase in the energy gap between the $S_2Q_A^{-\bullet}$/DCMU state and the $P_{680}^{+\bullet}Phe_{D1}^{-\bullet}$ state in PsbA2-PSII when compared to PsbA3-PSII can be estimated to be close to (27-15)/0.4 = 30 meV [64]. We have previously shown that the decay of the $S_1Tyr_Z^{\bullet}$ split EPR signal at 4.2 K in PsbA2-PSII was found similar to that in PsbA3-PSII [22]. This suggested that the driving forces for the charge recombination by the non-radiative direct route in the $S_1Tyr_Z^{\bullet}$-$Q_A^{-\bullet}$ state, *i.e.* a route that does not involve the repopulation of the $P_{680}^{+\bullet}Phe_{D1}^{-\bullet}$ state, was similar in PsbA2-PSII and PsbA3-PSII. Since, in addition, in the S_1 state the Tyr_Z oxidation by $P_{680}^{+\bullet}$ and the $Tyr_Z^{\bullet}$ reduction by the Mn_4CaO_5 cluster in the S_1-state remains almost unaffected in PsbA2-PSII, we proposed that the $E_m(Q_A/Q_A^{-\bullet})$ value in PsbA2-PSII was similar to that in PsbA3-PSII [22]. Therefore, the differences seen in the TL, *i.e.* an upshift of the peak temperature and a larger amplitude of the TL signal in PsbA2-PSII, are compatible with a lower E_m of $Phe_{D1}^{-\bullet}/Phe_{D1}$ as suggested in [25], [64]. Unfortunately, we have no data on the charge recombination at 4.2 K between the $S_2Tyr_Z^{\bullet}$ split EPR signal and $Q_A^{-\bullet}$ in PsbA2-PSII state because this split signal cannot be

formed in PsbA2-PSII even at room temperature (likely due to the change in the proton egress discussed above).

The Tyr_Z oxidation in the S_2 state at helium temperatures requires a pre-illumination at 200 K. In a computational study, it has been proposed that "the tautomerization of D1/Asn298 to its imidic acid form enables proton translocation to an adjacent asparagine-rich cavity of water molecules that functions as a proton reservoir and can further participate in proton egress to the lumen" [66]. Since the $S_2Tyr_Z^{\bullet}$ state can be formed upon an illumination at 200 K in PsbA3-PSII and PsbA1-PSII and not in PsbA2-PSII, the egress of the proton involved here may occur at 200 K and very likely the proton reservoir is constituted by the water molecules missing in PsbA2-PSII [25]. In addition, since D1/Asn298 is present in the three PsbA, it is not responsible for the loss of the capability of PsbA2-PSII to form the $S_2Tyr_Z^{\bullet}$ state.

The TL changes observed in PsbA2-PSII are partially reversed in PsbA2/M173P-PSII and partially induced in PsbA3/P173M-PSII. However, the lack of a symmetrical effect when we compare the data in the PsbA3-PSII *versus* those in the PsbA2/M173P-PSII on one hand and the data in the PsbA2-PSII *versus* those in the PsbA3/P173M-PSII on the other hand indicates that the other amino acid substitutions between PsbA2 and PsbA3 have an effect. Nevertheless, and in conclusion, the data in the present work are in good agreement with the deductions made from the crystal structures of PsbA2-PSII and PsbA3-PSII [26].

Characterizing the functional properties of PSII according to the nature of the D1 protein is the first step in understanding the advantage conferred by each of the D1 isoforms under the conditions where they are preferentially expressed. In PsbA3-PSII, which is up regulated under high light conditions [18], it was found that the less negative E_m value of the $Phe_{D1}^{-\bullet}/Phe_{D1}$ couple [18,28] could be responsible for a lower $^1O_2$ production [28]. Such a change is in agreement with a better resilience of PsbA3-PSII than PsbA1-PSII under high light conditions. However, if the *psbA*$_2$ transcription is strongly upregulated under micro-aerobic conditions [20], there is so far no quantification of the PsbA proteins in response to this stress and that remains to be done taking into account the possible complex regulation systems already identified in other cyanobacteria [67]. Assuming that PsbA2 is indeed produced under micro-aerobic conditions, a more negative E_m value of the $Phe_{D1}^{-\bullet}/Phe_{D1}$ couple in PsbA2-PSII than in PsbA1-PSII and PsbA3-PSII is expected to favor the formation of $^1O_2$ for all the reasons detailed in [28]. However, in the absence of O_2 the production of $^1O_2$ is no longer a problem. The fact that WT*2 cells are well growing in the presence of O_2 can be explained by the larger energy gap between the $Phe_{D1}Q_A^-$ state and the $Phe_{D1}^-Q_A$ state in

PsbA2-PSII than in PsbA1-PSII and PsbA3-PSII, which decreases the thermally activated repopulation of the $Phe_{D1}^{-}Q_A$ state and therefore favours the direct recombination at the expense of the triplet formation route [68].

Acknowledgements

This work has been in part supported by (i) the French Infrastructure for Integrated Structural Biology (FRISBI) ANR-10-INBS-05, (ii) the Labex Dynamo (ANR-11-LABX-0011-01) and (iii) the JSPS-KAKENHI Grant in Scientific Research on Innovative Areas JP17H064351 and a JSPS-KAKENHI Grant 21H02447. Bill Rutherford is acknowledged for a careful reading of the manuscript and Yuki Ito and Kosuke Tada for drawing figures.

References

1. Y. Umena, K. Kawakami, J-R. Shen, N. Kamiya, Crystal structure of oxygen-evolving Photosystem II at a resolution of 1.9 angstrom, Nature 473 (2011) 55–60. https://doi.org/10.1038/nature09913
2. H. Ago, H. Adachi, Y. Umena, T. Tashiro, K. Kawakami, N. Kamiya, L.R. Tian, G.Y. Han, T.Y. Kuang, Z.Y. Liu, F.J. Wang, H.F. Zou, I. Enami, M. Miyano, J-R. Shen, Novel features of eukaryotic photosystem II revealed by its crystal structure analysis from a red alga, J. Biol. Chem. 291 (2016) 5676–5687. https://doi.org/10.1074/jbc.M115.711689
3. C.J. Gisriel, J. Wang, J. Liu, D.A. Flesher, K.M. Reiss, H-L. Huang, K.R. Yang, W.H. Armstrong, M.R. Gunner, V.S. Batista, R.J. Debus, G.W. Brudvig, High-resolution cryo-electron microscopy structure of Photosystem II from the mesophilic cyanobacterium, *Synechocystis* sp. PCC 6803, Proc. Natl. Acad. Sci. USA 119 (2022) e2116765118. https://doi.org/10.1073/pnas.2116765118
4. I. Enami, A. Okumura, R. Nagao, T. Suzuki, M. Iwai, J-R. Shen, Structures and functions of the extrinsic proteins of photosystem II from different species, Photosynth. Res. 98 (2008) 349–363. https://doi.org/10.1007/s11120-008-9343-9
5. A.R. Holzwarth, M.G. Müller, M. Reus, M. Nowaczyk, J. Sander, M. Rögner, Kinetics and mechanism of electron transfer in intact Photosystem II and in the isolated reaction center: pheophytin is the primary electron acceptor, Proc. Natl. Acad. Sci. USA 103 (2006) 6895–6900. https://doi.org/10.1073/pnas.0505371103
6. F. Muh, M. Plockinger, T. Renger, Electrostatic asymmetry in the reaction center of Photosystem II, J. Phys. Chem. Lett. 8 (2017) 850−858. https://doi.org/10.1021/acs.jpclett.6b02823
7. D.J. Vinyard, G.M. Ananyev, G.C. Dismukes, Photosystem II: The Reaction center of oxygenic photosynthesis, Annu. Rev. Biochem. 82 (2013) 577–606. https://10.1146/annurev-biochem-070511-100425
8. D. Shevela, J.F. Kern, G. Govindjee, J. Messinger, Solar energy conversion by photosystem II: principles and structures, Photosynth. Res. Early access. https://doi.org/10.1007/s11120-022-00991-y
9. W. Lubitz, D.A. Pantazis, N. Cox, Water oxidation in oxygenic photosynthesis studied by magnetic resonance techniques, FEBS Lett. Early access. https://doi.org/10.1002/1873-3468.14543

10. N. Oliver, A.P. Avramov, D.J. Nürnberg, H. Dau, R.L. Burnap, From manganese oxidation to water oxidation: assembly and evolution of the water- splitting complex in photosystem II, Photosynth. Res. 152 (2022) 107–133. https://doi.org/10.1007/s11120-022-00912-z
11. T. Oliver, T.D. Kim, J.P. Trinugroho, V. Cordón-Preciado, N. Wijayatilake, A. Bhatia, A.W. Rutherford, T. Cardona, The evolution and evolvability of Photosystem II, Annu. Rev. Plant. Biol. 74 (2023) 24.1-24.33. https://doi.org/10.1146/annurev-arplant-070522-062509
12. P. Joliot, Period-four oscillations of the flash-induced oxygen formation in photosynthesis, Photosynth. Res. 76 (2003) 65–72. https://doi-org.insb.bib.cnrs.fr/10.1023/A:1024946610564
13. B. Kok, B. Forbush, M. McGloin, Cooperation of charges in photosynthetic O_2 evolution–I. A linear four step mechanism, Photochem. Photobiol. 11 (1970) 457–475. https://doi.org/10.1111/j.1751-1097.1970.tb06017.x
14. K. Yamaguchi, M. Shoji, H. Isobe, T. Kawakami, K. Miyagawa, M. Suga, F. Akita, J-R. Shen, Geometric, electronic and spin structures of the $CaMn_4O_5$ catalyst for water oxidation in oxygen-evolving photosystem II. Interplay between experiments and theoretical computations, Coord. Chem. Rev. 471 (2022) 214742. https://doi.org/10.1016/j.ccr.2022.214742
15. Y. Nakamura, T. Kaneko, S. Sato, M. Ikeuchi, H. Katoh, S. Sasamoto, A. Watanabe, M. Iriguchi, K. Kawashima, T. Kimura, Y. Kishida, C. Kiyokawa, M. Kohara, M. Matsumoto, A. Matsuno, N. Nakazaki, S. Shimpo, M. Sugimoto, C. Takeuchi, M. Yamada, S. Tabata, Complete genome structure of the thermophilic cyanobacterium *Thermosynechococcus elongatus* BP-1, DNA Res. 9 (2002) 123–130. https://10.1093/dnares/9.4.123
16. P. Mulo, C. Sicora, E.M. Aro, Cyanobacterial *psbA* gene family: optimization of oxygenic photosynthesis, Cell. Mol. Life Sci. 66 (2009) 3697–3710. https://doi.org/10.1007/s00018-009-0103-6
17. K.J. Sheridan, E.J. Duncan, J.J. Eaton-Rye, T.C. Summerfield, The diversity and distribution of D1 proteins in cyanobacteria, Photosynth. Res. 145 (2020) 111–128. https://doi.org/10.1007/s11120-020-00762-7
18. J. Sander, M. Nowaczyk, J. Buchta, H. Dau, I. Vass, Z. Deák, M. Dorogi, M. Iwai, M. Rögner, Functional characterization and quantification of the alternative PsbA copies in *Thermosynechococcus elongatus* and their role in photoprotection, J. Biol. Chem. 285 (2010) 29851–29856. https://doi.org/10.1074/jbc.M110.127142
19. P.B. Kós, Z. Deák, O. Cheregi, I. Vass, Differential regulation of *psbA* and *psbD* gene expression, and the role of the different D1 protein copies in the cyanobacterium

Thermosynechococcus elongatus BP-1, Biochim. Biophys. Acta, 1777 (2008) 74–83. https://doi.org/10.1016/j.bbabio.2007.10.015

20. C.I. Sicora, F.M. Ho, T. Salminen, S. Styring, E.-M. Aro, Transcription of a "silent" cyanobacterial *psbA* gene is induced by microaerobic conditions, Biochim. Biophys. Acta, 1787 (2009), 105–112. https://doi.org/10.1016/j.bbabio.2008.12.002
21. M. Sugiura, S. Ogami, M. Kusumi, S. Un, F. Rappaport, A. Boussac, Environment of Tyr_Z in Photosystem II from *Thermosynechococcus elongatus* in which PsbA2 is the D1 protein, J. Biol. Chem. 287 (2012) 13336–13347. https://doi.org/10.1074/jbc.M112.340323
22. A. Boussac, F. Rappaport, K. Brettel, M. Sugiura, Charge recombination in $S_nTyr_Z^{\bullet}Q_A^{-\bullet}$ radical pairs in D1 protein variants of Photosystem II: Long range electron transfer in the Marcus inverted region, J. Phys. Chem B. 117 (2013) 3308–3314. https://doi.org/10.1021/jp400337j
23. T. Motomura, M. Suga, R. Hienerwadel, A. Nakagawa, TL. Lai, W. Nitschke, T. Kuma, M. Sugiura, A. Boussac, J-R. Shen, Crystal structure and redox properties of a novel cyanobacterial heme protein with a His/Cys heme axial ligation and a Per-Arnt-Sim (PAS)-like domain, J. Biol. Chem. 292 (2017) 9599–9612. https://doi.org/10.1074/jbc.M116.746263
24. M. Sugiura, Y. Ozaki, M. Nakamura, N. Cox, F. Rappaport, A. Boussac, The D1-173 amino acid is a structural determinant of the critical interaction between D1-Tyr161 (Tyr_Z) and D1-His190 in Photosystem II, Biochim. Biophys. Acta 1837 (2014) 1922–1931. https://doi.org/10.1016/j.bbabio.2014.08.008
25. Y. Nakajima, N. Ugai-Amo, N. Tone, A. Nakagawa, M. Iwai, M. Ikeuchi, M. Sugiura, M. Suga, J-R. Shen, Crystal structures of photosystem II from a cyanobacterium expressing *psbA2* in comparison to *psbA3* reveal differences in the D1 subunit, J. Biol. Chem. 298 (2022) 102668. https://doi.org/10.1016/j.jbc.2022.102668
26. M. Sugiura, Y. Kato, R. Takahashi, H. Suzuki, T. Watanabe, T. Noguchi, F. Rappaport, A. Boussac, Energetics in Photosystem II from *Thermosynechococcus elongatus* with a D1 protein encoded by either the *psbA1* or *psbA3* gene, Biochim. Biophys. Acta 1797 (2010) 1491–1499. https://doi.org/10.1016/j.bbabio.2010.03.022
27. Y. Kato, M. Sugiura, A. Oda, T. Watanabe, Spectroelectrochemical determination of the redox potential of Pheophytin a, the primary electron acceptor in Photosystem II, Proc. Natl. Acad. Sci. U.S.A. 103 (2009) 17365–17370. https://doi.org/10.1073/pnas.0905388106
28. M. Sugiura, C. Azami, K. Koyama, A.W. Rutherford, F. Rappaport, A. Boussac, Modification of the pheophytin redox potential in *Thermosynechococcus elongatus*

Photosystem II with PsbA3 as D1, Biochim. Biophys. Acta 1837 (2014) 139–148. https://doi.org/10.1016/j.bbabio.2013.09.009

29. S.A.P. Merry, P.J. Nixon, L.M.C. Barter, M. Schilstra, G. Porter, J. Barber, J.R. Durrant, D.R. Klug, Modulation of quantum yield of primary radical pair formation in Photosystem II by site-directed mutagenesis affecting radical cations and anions, Biochemistry, 37 (1998) 17439–17447. https://doi.org/10.1021/bi980502d
30. M. Sugiura, A. Boussac, T. Noguchi, F. Rappaport, Influence of Histidine-198 of the D1 subunit on the properties of the primary electron donor, P680, of Photosystem II in *Thermosynechococcus elongatus*, Biochim. Biophys. Acta 1777 (2008) 331–342. https://doi.org/10.1016/j.bbabio.2008.01.007
31. M. Sugiura, Y. Inoue, Highly purified thermo-stable oxygen evolving Photosystem II core complex from the thermophilic cyanobacterium *Synechococcus elongatus* having His-tagged CP43. Plant Cell Physiol. 40 (1999)1219–1231. https://doi.org/10.1093/oxfordjournals.pcp.a029510
32. A. Boussac, M. Sugiura, J. Sellés, Probing the proton release by Photosystem II in the S_1 to S_2 high-spin transition, Biochim. Biophys. Acta 1863 (2022) 148546. https://doi.org/10.1016/j.bbabio.2022.148546
33. D. Béal, F. Rappaport, P. Joliot, A new high-sensitivity 10-ns time-resolution spectrophotometric technique adapted to in vivo analysis of the photosynthetic apparatus, Rev. Sci. Instrum. 70 (1999) 202–207. https://doi.org/10.1063/1.1149566
34. M. Sugiura, T. Taniguchi, N. Tango, M. Nakamura, J. Sellés, A. Boussac, Probing the role of arginine 323 of the D1 protein in Photosystem II function, Physiol. Plant. 171 (2021) 183–199. https://doi.org/10.1111/ppl.13115
35. A. Boussac, J. Sellés, M. Sugiura, What can we still learn from the electrochromic band-shifts in Photosystem II? Biochim. Biophys. Acta 1861 (2020) 148176. https://doi.org/10.1016/j.bbabio.2020.148176
36. J.-M. Ducruet, Chlorophyll thermoluminescence of leaf discs: simple instruments and progress in signal interpretation open the way to new ecophysiological indicators, J. Exp. Bot. 54 (2003) 2419–2430. https://doi.org/10.1093/jxb/erg268
37. J.-M. Ducruet, I. Vass, Thermoluminescence: experimental, Photosynth. Res. 201 (2009) 195–204. https://doi.org/10.1007/s11120-009-9436-0
38. M. Sugiura, T. Tibiletti, I. Takachi, Y. Hara, S. Kanawaku, J. Sellés, A. Boussac, Probing the role of Valine 185 of the D1 protein in the Photosystem II oxygen evolution, Biochim. Biophys. Acta 1859 (2018) 1259–1273. https://doi.org/10.1016/j.bbabio.2018.10.003

39. A. Klauss, M. Haumann, H. Dau, Seven steps of alternating electron and proton transfer in Photosystem II water oxidation traced by time-resolved photothermal beam deflection at improved sensitivity, J. Phys. Chem. B 119 (2015) 2677–2689. https://doi.org/10.1021/jp509069p

40. A. Boussac, M. Sugiura, F. Rappaport, Probing the quinone binding site of Photosystem II from *Thermosynechococcus elongatus* containing either PsbA1 or PsbA3 as the D1 protein through the binding characteristics of herbicides, Biochim. Biophys. Acta 1807 (2010) 119–129. https://doi.org/10.1016/j.bbabio.2010.10.004

41. P. Faller, R.J. Debus, K. Brettel, M. Sugiura, A.W. Rutherford, A. Boussac, Rapid formation of the stable tyrosyl radical in photosystem II, Proc. Natl. Acad. Sci. USA 98 (2001) 14368–14373. https://doi.org/10.1073/pnas.251382598

42. F. Rappaport, J. Lavergne, Proton release during successive oxidation steps of the photosynthetic water oxidation process - stoichiometries and pH-dependence, Biochemistry 30 (1991) 10004–10012. https://doi.org/10.1021/bi00105a027

43. M. Haumann, W. Junge, Extent and rate of proton release by photosynthetic water oxidation in thylakoids – electrostatic relaxation versus chemical production, Biochemistry 33 (1994) 864–872. https://doi.org/10.1021/bi00170a003

44. A. Klauss, T. Sikora, B. Süss, H. Dau, Fast structural changes (200–900 ns) may prepare the photosynthetic manganese complex for oxidation by the adjacent tyrosine radical, Biochim. Biophys. Acta 1817 (2012) 1196–1216. https://doi.org/10.1016/j.bbabio.2012.04.017

45. I. Zaharieva, H. Dau, M. Haumann, Sequential and coupled proton and electron transfer events in the $S_2 \rightarrow S_3$ transition of photosynthetic water oxidation revealed by time-resolved X-ray absorption spectroscopy, Biochemistry 55 (2016) 6996–7004. https://doi.org/10.1021/acs.biochem.6b01078

46. M. Mandal, K. Saito, H. Ishikita, Release of electrons and protons from substrate water molecules at the oxygen-evolving complex in Photosystem II, J. Phys. Soc. Jpn. 91 (2022) 091012. https://doi.org/10.7566/JPSJ.91.091012

47. T. Takaoka, N. Sakashita, K. Saito, H. Ishikita, pKa of a proton-conducting water chain in Photosystem II, J. Phys. Chem. Lett. 7 (2016) 1925–1932. https://doi.org/10.1021/acs.jpclett.6b00656

48. D. Kaur, Y. Zhang, K.M. Reiss, M. Mandal, G.W. Brudvig, V.S. Batista, M.R. Gunner, Proton exit pathways surrounding the oxygen evolving complex of photosystem II, Biochim. Biophys. Acta 1862 (2021) 148446. https://doi.org/10.1016/j.bbabio.2021.148446

49. R.J. Debus, FTIR studies of metal ligands, networks of hydrogen bonds, and water molecules near the active site Mn_4CaO_5 cluster in Photosystem II, Biochim. Biophys. Acta 1847 (2015) 19–34. https://doi.org/10.1016/j.bbabio.2014.07.007

50. M. Ibrahim, T. Fransson, R. Chatterjee, M.H. Cheah, R. Hussein, L. Lassalle, K.D. Sutherlin, I.D. Young, F.D. Fuller, S. Gul, I-S. Kim, P.S. Simon, C. de Lichtenberg, P. Chernev, I. Bogacz, C.C. Pham, A.M. Orville, N. Saichek, T. Northen, A. Batyuk, S. Carbajo, R. Alonso-Mori, K. Tono, S. Owada, A. Bhowmick, R. Bolotovsky, D. Mendez, N.W. Moriarty, J.M. Holton, H. Dobbek, A.S. Brewster, P.D. Adams, N.K. Sauter, U. Bergmann, A. Zouni, J. Messinger, J. Kern, V.K. Yachandra, J. Yano, Untangling the sequence of events during the $S_2 \rightarrow S_3$ transition in photosystem II and implications for the water oxidation mechanism, Proc. Natl. Acad. Sci. USA. 117 (2020)12624–12635. https://doi.org/10.1073/pnas.2000529117

51. Hussein R, Ibrahim M, Bhowmick A, Simon PS, Chatterjee R, Lassalle L, M. Doyle, I. Bogacz, I-S. Kim, M.H. Cheah, S. Gul, C. de Lichtenberg, P. Chernev, C.C. Pham, I.D. Young, S. Carbajo, F.D. Fuller, R. Alonso-Mori, A. Batyuk, K.D. Sutherlin, A.S. Brewster, R. Bolotovsky, D. Mendez, J. M. Holton, N.W. Moriarty, P.D. Adams, U. Bergmann, N.K. Sauter, H. Dobbek, J. Messinger, A. Zouni, J. Kern, V.K. Yachandra, J. Yano, Structural dynamics in the water and proton channels of photosystem II during the S_2 to S_3 transition. Nat. Commun. 12 (2021) 6531. https://doi.org/10.1038/s41467-021-26781-z

52. Y. Okamoto, Y. Shimada, R. Nagao, T. Noguchi, Proton and water transfer pathways in the $S_2 \rightarrow S_3$ transition of the water-oxidizing complex in Photosystem II: Time-resolved infrared analysis of the effects of D1-N298A mutation and NO_3^- substitution, J. Phys. Chem. B 125 (2021) 6864–6873. https://doi.org/10.1021/acs.jpcb.1c03386

53. Y. Shimada, A. Sugiyama, R. Nagao, T. Noguchi, Role of D1-Glu65 in proton transfer during photosynthetic water oxidation in Photosystem II, J. Phys. Chem. B 126 (2022) 8202–8213. https://doi.org/10.1021/acs.jpcb.2c05869

54. V. Krewald, M. Retegan, N. Cox, J. Messinger, W. Lubitz, S. DeBeer, F. Neese, D.A. Pantazis, Metal oxidation states in biological water splitting, Chem. Sci., 6 (2015) 1676–1695. https://doi.org/10.1039/c4sc03720k

55. K. Saito, A.W. Rutherford, H. Ishikita, Energetics of proton release on the first oxidation step in the water-oxidizing enzyme, Nat Commun 6 (2015) 8488. https://doi.org/10.1038/ncomms9488

56. T. Shimizu, M. Sugiura, T. Noguchi, Mechanism of proton-coupled electron transfer in the S_0-to-S_1 transition of photosynthetic water oxidation as revealed by time-resolved infrared

spectroscopy, J. Phys. Chem. B 122 (2018) 9460–9470. https://doi.org/10.1021/acs.jpcb.8b07455

57. P.E.M. Siegbahn, Water oxidation mechanism in Photosystem II, including oxidations, proton release pathways, O—O bond formation and O_2 release, Biochim. Biophys. Acta 1827 (2013) 1003–1019. http://dx.doi.org/10.1016/j.bbabio.2012.10.006
58. M. Retegan, N. Cox, W. Lubitz, F. Neese, D.A. Pantazis, The first tyrosyl radical intermediate formed in the S2-S3 transition of photosystem II, Phys. Chem. Chem. Phys. 16 (2014) 11901–11910. https://doi.org/10.1039/c4cp00696h
59. D. Narzi, D. Bovi, L. Guidoni, Pathway for Mn-cluster oxidation by tyrosine-Z in the S_2 state of photosystem II, Proc. Nat. Aca. Sci. USA, 111 (2014), pp. 8723–8728. https://doi.org/10.1073/pnas.1401719111
60. P.E.M. Siegbahn, The S_2 to S_3 transition for water oxidation in PSII (photosystem II), revisited, Phys. Chem. Chem. Phys. 20 (2018) 22926–22931. https://doi.org/10.1039/C8CP03720E
61. C. Berthomieu, R. Hienerwadel, Iron coordination in photosystem II: Interaction between bicarbonate and the Q_B pocket studied by Fourier transform infrared spectroscopy, Biochemistry 40 (2001) 4044–4052. https://doi.org/10.1021/bi002236l
62. Y. Kato, T. Noguchi, Redox properties and regulatory mechanism of the iron-quinone electron acceptor in photosystem II as revealed by FTIR spectroelectrochemistry, Photosynth. Res. 152 (2022) 135–151. https://doi.org/10.1007/s11120-021-00894-4.
63. H. Ishikita, E.-W. Knapp, Oxidation of the non-heme iron complex in Photosystem II, Biochemistry 44 (2005) 14772–14783. https://doi.org/10.1021/bi051099v
64. F. Rappaport, J. Lavergne, Thermoluminescence: theory, Photosynth. Res. 101 (2009) 205–216. https://doi.org/10.1007/s11120-009-9437-z
65. K. Cser, I. Vass, Radiative and non–radiative charge recombination pathways in Photosystem II studied by thermoluminescence and chlorophyll fluorescence in the cyanobacterium *Synechocystis* 6803, Biochim. Biophys. Acta 1767 (2007) 233–243. https://doi.org/10.1016/j.bbabio.2007.01.022
66. M. Chrysina, J.C. de Mendonça Silva, G. Zahariou, D.A. Pantazis, N. Ioannidis, Proton translocation *via* tautomerization of Asn298 during the S_2–S_3 State transition in the oxygen-evolving complex of Photosystem II, J. Phys. Chem. B 123 (2019) 3068–3078. https://doi.org/10.1021/acs.jpcb.9b02317

67. P. Mulo, I. Sakurai, E-M. Aro, Strategies for *psbA* gene expression in cyanobacteria, green algae and higher plants: From transcription to PSII repair, Biochim. Biophys. Acta 1817 (2012) 247–257. https://doi.org/10.1016/j.bbabio.2011.04.011

68. A.W. Rutherford, A. Osyczka, F. Rappaport, Back-reactions, short-circuits, leaks and other energy wasteful reactions in biological electron transfer: Redox tuning to survive life in O_2, FEBS Lett. 586 (2012) 603–616. https://doi.org/10.1016/j.febslet.2011.12.039

Table 1: $t_{1/2}$ values resulting from the fits of the kinetics in Fig. 2.

	1st flash	2nd flash ($S_2Tyr_Z^{\bullet} \rightarrow S_3Tyr_Z$)	3rd flash ($S_3Tyr_Z^{\bullet} \rightarrow S_0Tyr_Z$)	4th flash ($S_0Tyr_Z^{\bullet} \rightarrow S_1Tyr_Z$)
PsbA3	317 µs	48 µs	30 µs / 1.9 ms	212 µs
PsbA2	678 µs	93 µs	76 µs / 1.6 ms	88 µs / 1.9 ms (global ~ 200 µs)
PsbA3-P173M	833 µs	77 µs	91 µs / 2.1 ms	101 µs
PsbA2-M173P	440 µs	50 µs	47 µs / 1.7 ms	52 µs / 373 µs (global ~ 100 µs)

Legends of Figures

Figure 1: Structural changes between PsbA2-PSII and PsbA3-PSII investigated in the present study. The drawing was done with Mac PyMol 2.5.0 by using the PDB structure 7yq2 for PsbA2-PSII and 7yq7 for PsbA3-PSII [25]. Labels in red characters identify the amino acid residues that differs in PsbA1, PsbA2 and PsbA3.

Figure 2: Time-courses of the absorption changes of bromocresol purple at 575 nm at pH 6.3 with PsbA3-PSII (Panel A), replotted from [36], PsbA2-PSII (Panel B), PsbA3/P173M-PSII (Panel C), and PsbA2/M173P-PSII (Panel D). The measurements were done after the 1^{st} (black points), the 2^{nd} (red points), the 3^{rd} (blue points) and the 4^{th} (green points) flashes given on dark-adapted PSII. The continuous lines are the fits of the data using exponential functions. For the 1^{st} flash in PsbA2-PSII, PsbA3/P173M-PSII and PsbA2/M173P-PSII the first data points were not taken into account in the fitting procedure.

Figure 3: Time-courses of the absorption change differences 440 nm-*minus*-424 nm after the 1^{st} flash (black), the 2^{nd} flash (red), the 3^{rd} flash (blue), and the 4^{th} flash (green) given to either dark-adapted PsbA3-PSII (Panel A) or PsbA2-PSII (Panel B).

Figure 4: Thermoluminescence curves from $S_2Q_A^-$/DCMU charge recombination measured after one flash given at -10°C in PsbA3-PSII (black points), PsbA2-PSII (blue points), PsbA3/P173M-PSII (red points) and PsbA2-M173P-PSII (green points). The heating rate was 0.4°C/s.

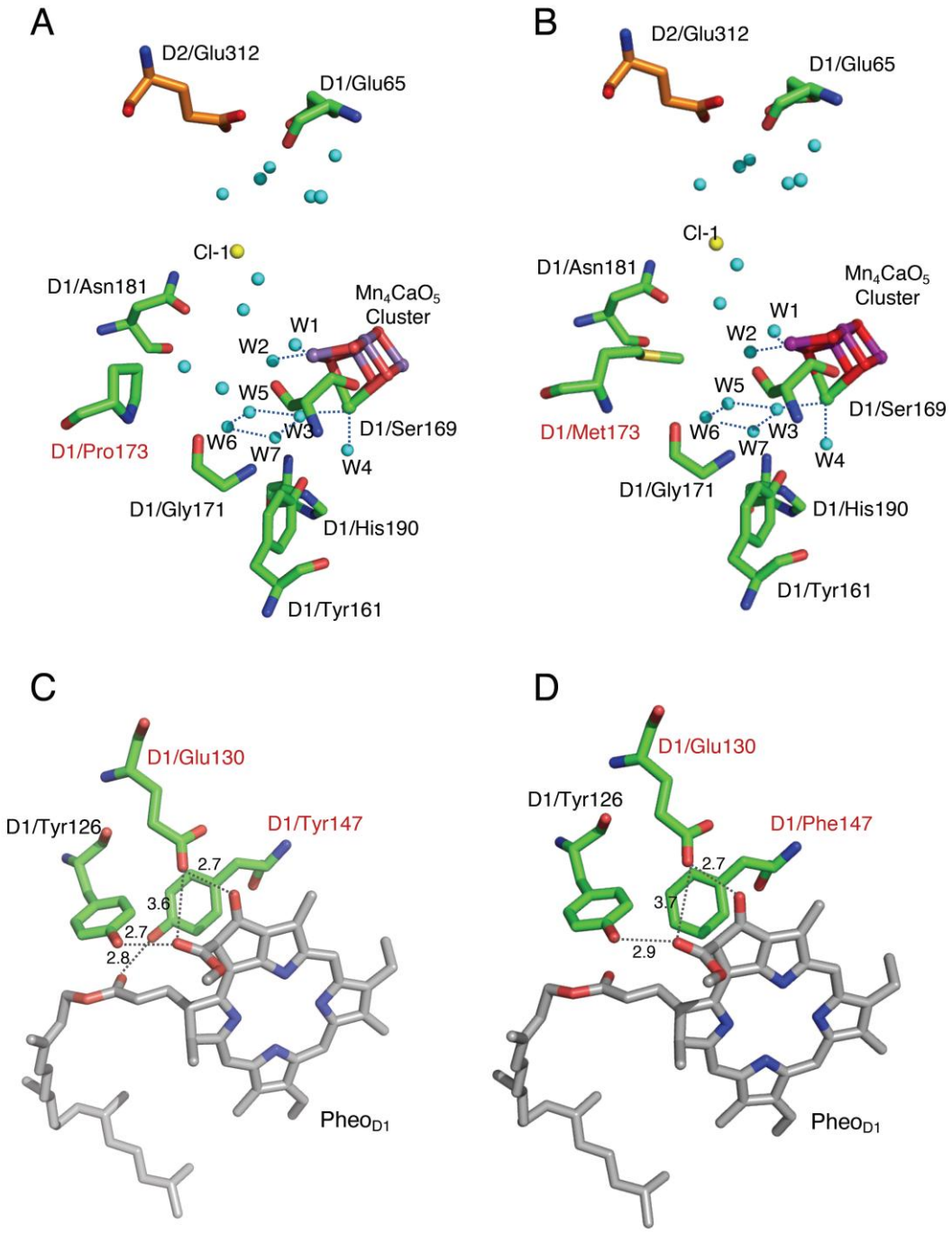
A
D2/Glu312
D1/Glu65
Cl-1
D1/Asn181
Mn4CaO5 Cluster
W1
W2
W5
W6
W3
W7
W4
D1/Ser169
D1/Pro173
D1/Gly171
D1/His190
D1/Tyr161
B
D2/Glu312
D1/Glu65
Cl-1
D1/Asn181
Mn4CaO5 Cluster
W1
W2
W5
D1/Ser169
D1/Met173
W6
W3
W7
W4
D1/Gly171
D1/His190
D1/Tyr161
C
D1/Glu130
D1/Tyr126
D1/Tyr147
2.7
3.6
2.7
2.8
PheoD1
D
D1/Glu130
D1/Tyr126
D1/Phe147
2.7
3.7
2.9
PheoD1

Fig.

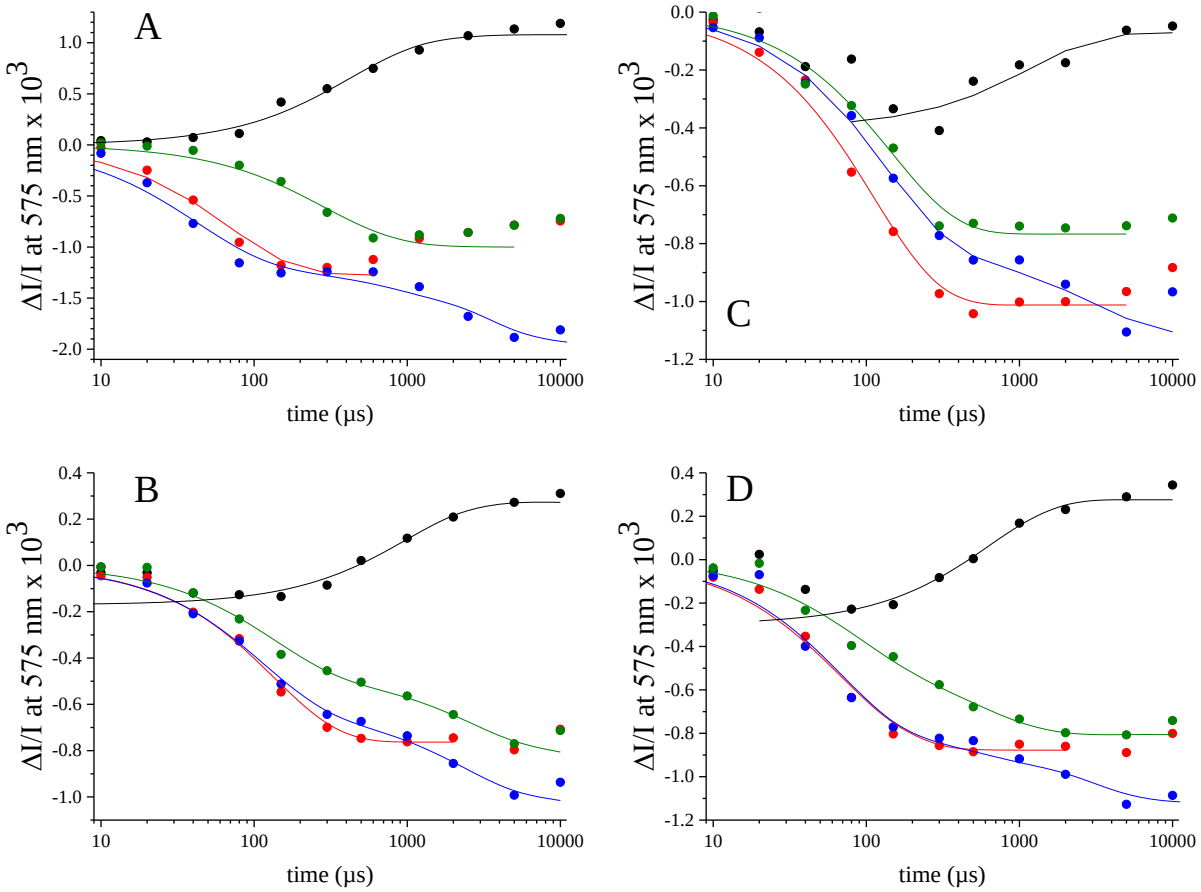

Fig. 2

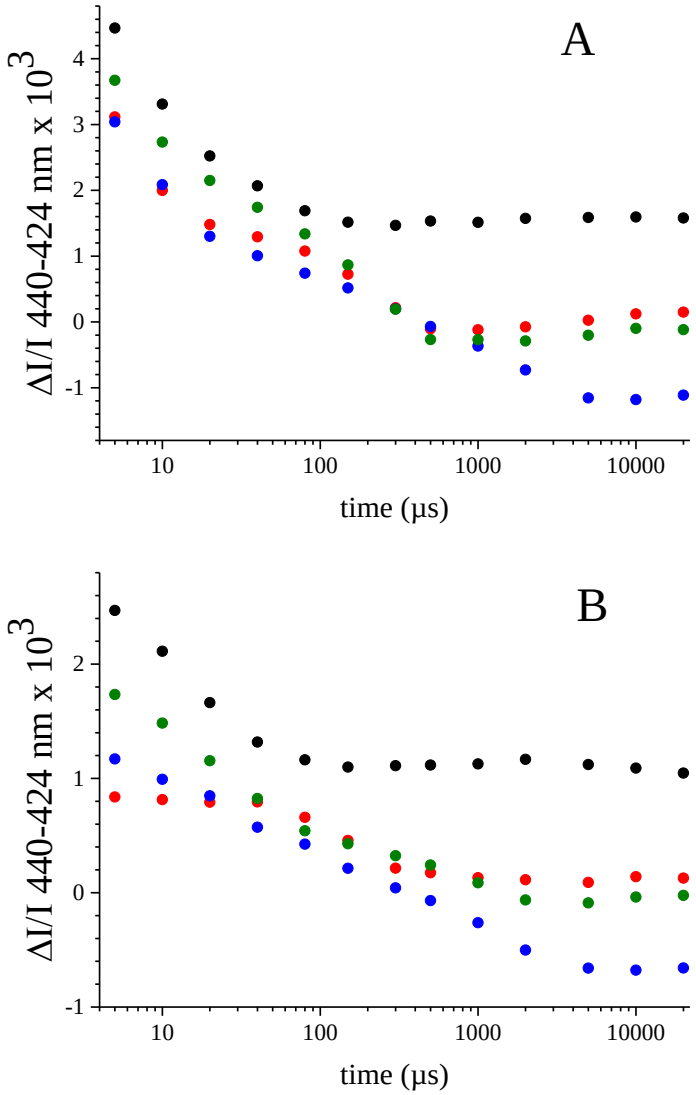
A
ΔI/I 440-424 nm x 10^3
4
3
2
1
0
-1
10
100
1000
10000
time (μs)
B
ΔI/I 440-424 nm x 10^3
2
1
0
-1
10
100
1000
10000
time (μs)

Fig. 3

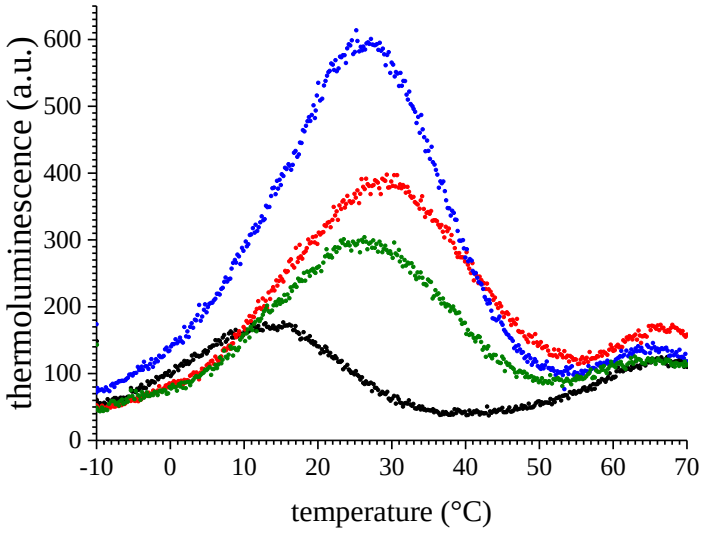
thermoluminescence (a.u.)
0
100
200
300
400
500
600
-10
0
10
20
30
40
50
60
70
temperature (°C)

Fig. 4